

# Numerical algorithms for spatial registration of line fiducials from cross-sectional images

Sangyoon Lee

*Department of Mechanical Engineering, The Johns Hopkins University, Baltimore, Maryland 21218*

Gabor Fichtinger

*Center for Computer-Integrated Surgical Systems and Technology, The Johns Hopkins University, Baltimore, Maryland 21218*

Gregory S. Chirikjian<sup>a)</sup>

*Department of Mechanical Engineering, The Johns Hopkins University, Baltimore, Maryland 21218*

(Received 22 October 2001; accepted for publication 9 May 2002; published 29 July 2002)

We present several numerical algorithms for six-degree-of-freedom rigid-body registration of line fiducial objects to their marks in cross-sectional planar images, such as those obtained in CT and MRI, given the correspondence between the marks and line fiducials. The area of immediate application is frame-based stereotactic procedures, such as radiosurgery and functional neurosurgery. The algorithms are also suitable to problems where the fiducial pattern moves inside the imager, as is the case in robot-assisted image-guided surgical applications. We demonstrate the numerical methods on clinical CT images and computer-generated data and compare their performance in terms of robustness to missing data, robustness to noise, and speed. The methods show two unique strengths: (1) They provide reliable registration of incomplete fiducial patterns when up to two-thirds of the total fiducials are missing from the image; and (2) they are applicable to an arbitrary combination of line fiducials without algorithmic modification. The average speed of the fastest algorithm is 0.3236 s for six fiducial lines in real CT data in a Matlab implementation.

© 2002 American Association of Physicists in Medicine. [DOI: 10.1118/1.1493777]

Key words: stereotactic registration, line fiducials, numerical algorithms, robustness

## I. INTRODUCTION

In this paper, we present several numerical methods for rigid body coregistration of line fiducials and their corresponding cross-sectional image, such as a CT or MRI image slice. Our work originates from frame-based stereotactic procedures, such as stereotactic radiosurgery and functional neurosurgery. Traditional stereotactic registration algorithms have an excellent track record in these applications, where the frame is rigidly fixed to the patient and only preoperative imaging is used. At the same time, however, classic registration methods begin to show their limits when used outside the scope of their original design. In this paper we discuss new challenges for frame-based stereotactic registration and present alternative computational methods to solve those problems.

Stereotactic head frames have been used for over two decades. Initial applications were intracranial neurosurgery and radiosurgery.<sup>1-3</sup> The methodology has been further extended for extracranial radiotherapy applications,<sup>4-7</sup> and then recently for robotically assisted surgery.<sup>8,9</sup> Popular registration algorithms follow the theme described by Brown<sup>1</sup> and many years later by Susil<sup>10</sup> and Masamune.<sup>9</sup> Classic stereotactic fiducial frames are composed of nine fiducial rods, which are arranged in three N-shaped motifs. Some of the frequently used stereotactic fiducial frames are shown in Fig. 1. These head frames are highly redundant fiducials that provide robustness against image processing errors. The strength of these registration systems is the ability to achieve concurrent

registration and target definition from a single image slice using a simple calculation with a closed formula. The pioneers of stereotaxy (Brown, Kelly, Leksell *et al.*)<sup>1-3</sup> were successful in maximizing accuracy while still minimizing computational complexity. These registration systems have served reliably in classic applications where the frame is rigidly attached to the body and the imaging protocol is strictly controlled in a preoperative session. Emerging intraoperative imaging, however, presents new challenges.

Classic registration methods uniformly fail when the pattern of fiducials is incomplete, i.e., when certain rods are missing from the cross-sectional image. This problem has always been present in frame-based stereotactic navigation, but it became critical with the advance of fast imaging scanners, allowing for intraoperative stereotactic navigation. In these applications, the stereotactic frame is not necessarily attached to the patient, allowing for greater maneuverability. As a result, the fiducial frame can move outside the field of view during the procedure, causing fiducial rods to be missing from the image. In robotically assisted surgery, the end-effector of a robot can be registered to the scanner using a rigid body fiducial frame attached to the end-effector. Susil<sup>10</sup> suggested a miniature version of a stereotactic head frame. Masamune<sup>8,9</sup> built the first clinically applicable embodiment of Susil's prototype. Susil's device and Masamune's device are displayed in Figs. 2(a) and 2(b), respectively. Early experience with Masamune's device revealed<sup>11</sup> that the incompleteness of data tends to be a chronic problem because it is

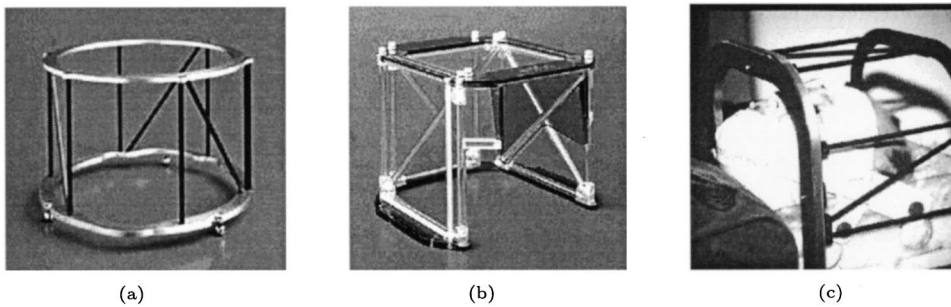


FIG. 1. Some of the frequently used stereotactic fiducial frames. (a) BRW CT. (b) BRW MRI. (c) Kelly CT.

common for the robot to accidentally move the fiducial frame out of the field of view, causing the image slice to become incomplete for registration. Figure 3 illustrates an image of Masamune's device with an incomplete number of fiducial rods. Traditional methods cannot handle this problem without acquiring extra images, which costs time and exposes the patient to unnecessary radiation.

Classic registration algorithms must be "reinvented" each time when the geometric description of the frame (shape, assembly of rods, etc.) changes. This is particularly inconvenient when one needs to go through several prototypes of a new design. Image-guided robots must often work in tight spaces like inside the gantry of a CT, where there may not be sufficient room for a conventional fiducial device composed of a triplet of V- or N-shaped planar motifs.

The foregoing problems could be eliminated by a computational method that is invariant to the number and assembly of fiducials in the stereotactic frame. In this generic scenario, conventional fiducial devices like the Brown–Roberts–Wells<sup>1</sup> or Kelly<sup>2</sup> head frames in Fig. 1 are uniformly handled, and incomplete scans also fit in the framework.

There are additional requirements for a new registration method. Very importantly, it must be resistant to noise in the input data. One of the inputs to the registration algorithm is the two-dimensional coordinates of the fiducial marks in the cross-sectional image. This information is produced by an image processing program that is not the subject of this investigation. It is conceivable that the locations of fiducial marks are not exactly identified in the medical images, due to suboptimal imaging and image processing techniques. These errors are considered to be "noise" in the input to the registration algorithm.

As we mentioned earlier, in many applications a single slice must be sufficient for full (six degrees-of-freedom) registration. Other works have been performed with other criteria in mind. For instance, Zylka *et al.*<sup>12</sup> assumed that all the image slices have been acquired without motion of the head frame between image slices (all slices were parallel), and they registered the lines from the 3-D volume of image data to the head frame. They, however, did not solve the problem of registering planar point patterns to lines in space; therefore their approach is not applicable to single-slice-based registration.

The algorithms sought must also run reasonably fast, in order to be useful in intraoperative applications. Computation time longer than one second would be prohibitive.

The mathematical problem in this paper is basically to register a planar image in space, given a set of known lines in space, given a pattern of points in the plane, and given a correspondence between the lines and points. Figure 4 displays Masamune's device when seven intersection points are generated in an image plane. While the problem of registering one set of points to another has received a lot of attention, the general problem of registering points to lines has not been studied as extensively.<sup>14</sup> There are two variants of this problem that are addressed here. In the first, we are interested in finding the equation of the plane. If we know this, then the planar registration of one planar set of points to the other can be performed afterward. In the second formulation of the problem, a frame of reference is attached to the intersecting plane, and we solve for the position and orientation of this frame in three-dimensional space. Hence, in the first approach two three-parameter problems are solved sequentially, while in the second approach one six-parameter problem is solved.

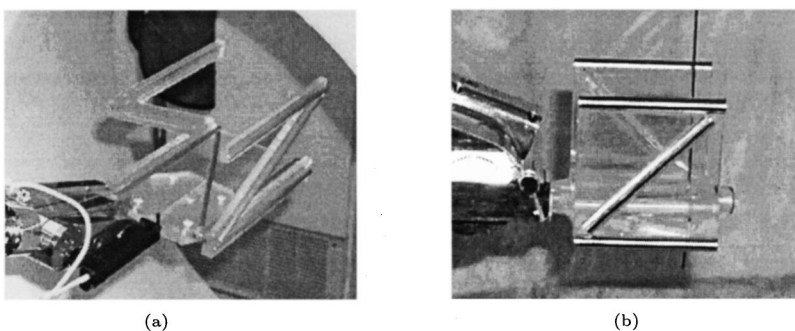


FIG. 2. Stereotactic localizers mounted on robotic needle drivers. (a) Susil's device. (b) Masamune's device.

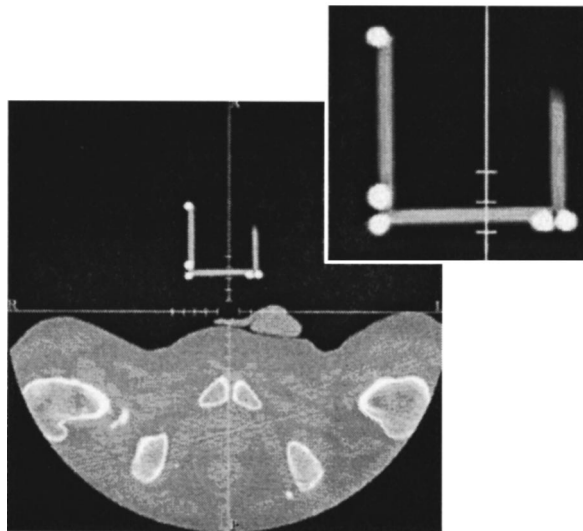


FIG. 3. Example of incomplete data with the Masamune's device.

We present several algorithms for both mathematical approaches. We demonstrate the numerical methods on clinical CT images and computer-generated data. We compare their performance in terms of robustness to missing data, robustness to noise, and speed. We implemented our algorithms as Matlab programs to prove the computational feasibility.

**II. MATHEMATICAL BACKGROUND AND NOTATION**

In this section we review the fundamental mathematics of lines in space and rigid-body motions to the extent needed to formulate and solve the registration problems presented later in this paper.

**A. Parametric description of lines in space**

The position of points in three-dimensional space are denoted with vectors  $\mathbf{x}=[x_1,x_2,x_3]^T \in \mathbb{R}^3$ , where the superscript  $T$  denotes the transpose of a vector or a matrix. A line in space is defined by the position of any point through

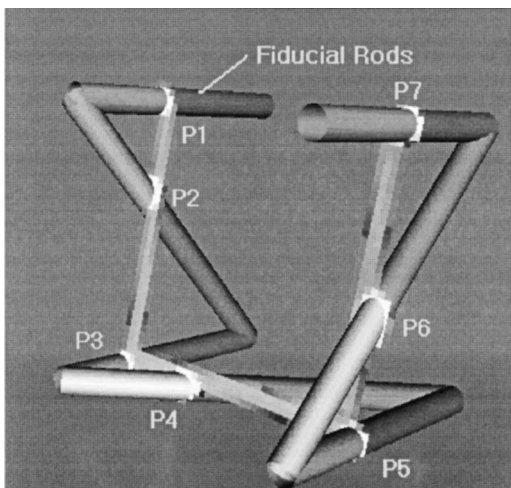


FIG. 4. Seven points ( $P_1-P_7$ ) are generated by intersecting the image plane.

which the line passes, together with a unit vector specifying the direction of the line. In parametric form, a line is given by the equation

$$\mathbf{x}(s) = \mathbf{p} + s\mathbf{v}, \tag{1}$$

where  $s$  is the distance along the line measured from the point  $\mathbf{p}$ , and  $\mathbf{v}$  is the unit vector specifying the direction of the line. Given multiple lines,  $\mathbf{x}_1(s_1), \dots, \mathbf{x}_n(s_n)$ , the  $i$ th will be defined by the vectors  $\mathbf{p}_i$  and  $\mathbf{v}_i$ .

**B. Review of rigid-body kinematics**

A spatial rigid-body motion consists of a rotation and a translation which act on a position vector as

$$\mathbf{x}' = R\mathbf{x} + \mathbf{b},$$

where  $\mathbf{x}, \mathbf{x}', \mathbf{b} \in \mathbb{R}^3$  and  $R \in SO(3)$  (the three-dimensional rotation group). The pair  $g = (R, \mathbf{b}) \in SO(3) \times \mathbb{R}^3$  describes both motion of a rigid body and the relationship between reference frames fixed in space and in the body. Furthermore, motions characterized by a pair  $(R, \mathbf{b})$  could either describe the behavior of a rigid body or of a deformable object undergoing a rigid-body motion during the time interval for which this description is valid.

Consider a rigid-body motion that moves a reference frame originally coincident with the "natural" space-fixed frame  $(I, \mathbf{0})$  to  $(R_1, \mathbf{b}_1)$ . Now consider a relative motion of the frame  $(R_2, \mathbf{b}_2)$  with respect to the frame  $(R_1, \mathbf{b}_1)$ . That is, given any vector  $\mathbf{x}$  defined in the terminal frame, it will look like  $\mathbf{x}' = R_2\mathbf{x} + \mathbf{b}_2$  in the frame  $(R_1, \mathbf{b}_1)$ . Then the same vector will appear in the natural frame as

$$\mathbf{x}'' = R_1(R_2\mathbf{x} + \mathbf{b}_2) + \mathbf{b}_1 = R_1R_2\mathbf{x} + R_1\mathbf{b}_2 + \mathbf{b}_1.$$

The net effect of composing the two motions (or changes of reference frame) is equivalent to the definition

$$(R_3, \mathbf{b}_3) = (R_1, \mathbf{b}_1) \circ (R_2, \mathbf{b}_2) \triangleq (R_1R_2, R_1\mathbf{b}_2 + \mathbf{b}_1). \tag{2}$$

From this expression, we can calculate the motion  $(R_2, \mathbf{b}_2)$  that for any  $(R_1, \mathbf{b}_1)$  will return the body-fixed frame to the space-fixed frame. All that is required is to solve  $R_1R_2 = I$  and  $R_1\mathbf{b}_2 + \mathbf{b}_1 = \mathbf{0}$  for the variables  $R_2$  and  $\mathbf{b}_2$  and given  $R_1$  and  $\mathbf{b}_1$ . The result is  $R_2 = R_1^T$  because  $R^{-1} = R^T$  for  $R \in SO(3)$  and  $\mathbf{b}_2 = -R_1^T\mathbf{b}_1$ . Thus, we denote the inverse of a motion as

$$(R, \mathbf{b})^{-1} = (R^T, -R^T\mathbf{b}). \tag{3}$$

This inverse, when composed either on the left or the right side of  $(R, \mathbf{b})$ , yields  $(I, \mathbf{0})$ .

The set of all pairs  $(R, \mathbf{b})$ , together with the operation  $\circ$ , is denoted as  $SE(3)$ , which is the three-dimensional rigid-body motion group. It is often convenient to represent elements of this group using  $4 \times 4$  homogeneous transformation matrices:

$$H(R, \mathbf{b}) = \begin{pmatrix} R & \mathbf{b} \\ \mathbf{0}^T & 1 \end{pmatrix}.$$

Left and right differential operators  $\tilde{X}_i^L$  and  $\tilde{X}_i^R$  for  $i = 1, \dots, 6$  acting on functions on  $SE(3)$  are defined in analogy with the definition of the partial derivative (or directional

derivative) of a complex-valued function of  $\mathbb{R}^N$ -valued argument. For small displacements from the identity,  $I$ , along or about a coordinate axis, the homogeneous transforms representing infinitesimal motions look like

$$H_i(\epsilon) \triangleq \exp(\epsilon \tilde{E}_i) \approx I + \epsilon \tilde{E}_i,$$

where  $i = 1, 2, 3$  and  $i = 4, 5, 6$ , respectively, correspond to rotations or translations for  $x$ ,  $y$ , and  $z$  axes and

$$\tilde{E}_1 = \begin{pmatrix} 0 & 0 & 0 & 0 \\ 0 & 0 & -1 & 0 \\ 0 & 1 & 0 & 0 \\ 0 & 0 & 0 & 0 \end{pmatrix}; \quad \tilde{E}_2 = \begin{pmatrix} 0 & 0 & 1 & 0 \\ 0 & 0 & 0 & 0 \\ -1 & 0 & 0 & 0 \\ 0 & 0 & 0 & 0 \end{pmatrix};$$

$$\tilde{E}_3 = \begin{pmatrix} 0 & -1 & 0 & 0 \\ 1 & 0 & 0 & 0 \\ 0 & 0 & 0 & 0 \\ 0 & 0 & 0 & 0 \end{pmatrix}; \quad \tilde{E}_4 = \begin{pmatrix} 0 & 0 & 0 & 1 \\ 0 & 0 & 0 & 0 \\ 0 & 0 & 0 & 0 \\ 0 & 0 & 0 & 0 \end{pmatrix};$$

$$\tilde{E}_5 = \begin{pmatrix} 0 & 0 & 0 & 0 \\ 0 & 0 & 0 & 1 \\ 0 & 0 & 0 & 0 \\ 0 & 0 & 0 & 0 \end{pmatrix}; \quad \tilde{E}_6 = \begin{pmatrix} 0 & 0 & 0 & 0 \\ 0 & 0 & 0 & 0 \\ 0 & 0 & 0 & 1 \\ 0 & 0 & 0 & 0 \end{pmatrix}.$$

Given that elements of  $SE(3)$  (viewed as homogeneous transforms) are parametrized as  $H = H(\mathbf{q})$ , where  $\mathbf{q}$  is a six-dimensional array of rotation and translation parameters, differential operators take the form

$$\begin{aligned} \tilde{X}_i^R f(H) &= \lim_{\epsilon \rightarrow 0} \frac{1}{\epsilon} [f(H \circ H_i(\epsilon)) - f(H)] \\ &= \left. \frac{df(H \circ (I + t\tilde{E}_i))}{dt} \right|_{t=0}, \end{aligned} \tag{4}$$

$$\begin{aligned} \tilde{X}_i^L f(H) &= \lim_{\epsilon \rightarrow 0} \frac{1}{\epsilon} [f(H_i^{-1}(\epsilon) \circ H) - f(H)] \\ &= \left. \frac{df((I - t\tilde{E}_i) \circ H)}{dt} \right|_{t=0}. \end{aligned} \tag{5}$$

Since  $H$  and  $H_i(\epsilon)$  are  $4 \times 4$  matrices, we henceforth drop the “ $\circ$ ” notation since it is understood as matrix multiplication.

If we want to analytically minimize a function of rigid-body motion,  $f(H)$ , we set

$$\tilde{X}_i^R f(H) = 0$$

or

$$\tilde{X}_i^L f(H) = 0,$$

for  $i = 1, \dots, 6$  and solve the resulting six equations. If we want to minimize  $f(H)$  numerically, we do gradient descent by using a numerical approximation to Eq. (4) or Eq. (5). For example, if for small values of  $\epsilon$ ,

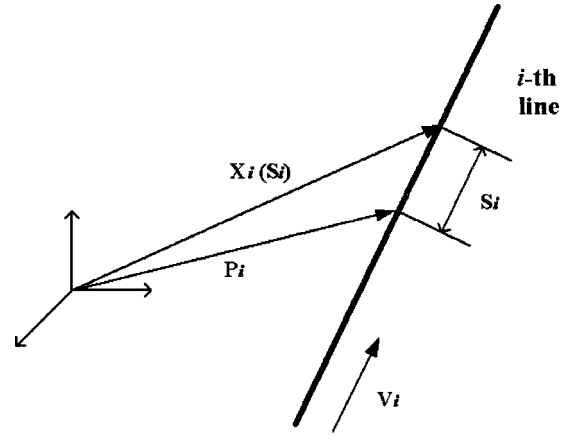


FIG. 5. Mathematical parameters of a line.

$$\tilde{X}_i^R f(H) \approx \frac{1}{\epsilon} [f(H \cdot H_i(\epsilon)) - f(H)],$$

is negative, then this indicates that this is a favorable direction in which to update the rigid-body motion as  $H \rightarrow H \cdot (I + \epsilon \tilde{E}_i)$ . If it is positive, then update as  $H \rightarrow H \cdot (I - \epsilon \tilde{E}_i)$ . If it is close to zero, then do not update in this direction. This process is repeated by cycling through values of subscript  $i$  until a minimum is reached.

### III. NUMERICAL METHODS

#### A. Solving a system of polynomials (algorithm 1)

The technique presented in this section uses Eq. (1) to find the plane in space in which the image must lie. After this plane is found, existing point-to-point registration techniques are used to determine the rigid-body motion between frames.

#### 1. Determination of the image plane in space

Suppose we are given a head frame with three fiducial lines and three corresponding fiducial points in the planar image. The problem of finding the location of the image plane in space can be solved by simultaneously satisfying three constraint equations of the form

$$\|\mathbf{x}_i(s_i) - \mathbf{x}_j(s_j)\|^2 = d_{ij}^2, \tag{6}$$

for  $(i, j) \in \{(1, 2), (1, 3), (2, 3)\}$ . In general, if more than three fiducials are used, this problem is overdetermined, so only an approximate solution is possible. As shown in Fig. 5,  $\mathbf{x}_i(s_i)$  is a position vector of a point on the  $i$ th line that is defined by the position  $\mathbf{p}_i$  and unit direction  $\mathbf{v}_i$ . Here  $s_i$  is the arclength from  $\mathbf{p}_i$  to  $\mathbf{x}_i(s_i)$  and  $d_{ij}$  is the Euclidean distance between  $\mathbf{x}_i(s_i)$  and  $\mathbf{x}_j(s_j)$ .

This set of equations will, in general, be a second-order polynomial in  $s_i$  and  $s_j$  of the form

$$s_i^2 - 2s_i s_j \cos \theta_{ij} + s_j^2 + a_{ij} s_i + b_{ij} s_j = d_{ij}^2 + c_{ij}.$$

The constants  $a_{ij}$ ,  $b_{ij}$ ,  $\theta_{ij}$ , and  $c_{ij}$  all come from the geometry of the problem and  $\cos \theta_{ij} = \mathbf{v}_i \cdot \mathbf{v}_j$ .

The approach we take is to iteratively solve the system of polynomials by assuming that each of the parameters can

vary with “artificial” time. We make an initial guess  $s_i(0)$  (in practice, this guess corresponds to the plane whose normal is the axis of the head frame with a value of  $c_{ij}$  that causes this plane to cut the head frame in half).

Then we take the time derivative to get

$$2s_i\dot{s}_i - 2(\dot{s}_i s_j + s_i \dot{s}_j) \cos \theta_{ij} + 2s_j \dot{s}_j + a_{ij} \dot{s}_i + b_{ij} \dot{s}_j = 2d_{ij} \dot{d}_{ij}. \tag{7}$$

The right-hand side follows from the fact that  $c_{ij}$  is a constant. We can assemble the three equations of the form in Eq. (7) as

$$J(\mathbf{s})\dot{\mathbf{s}} = \mathbf{w}. \tag{8}$$

The problem does not dictate the behavior of  $\dot{d}_{ij}$  in the mathematical model. However, if we specify

$$\dot{d}_{ij} = (d_{ij})_{\text{measured}} - d_{ij},$$

where  $(d_{ij})_{\text{measured}}$  denotes the Euclidean distance between the  $i$ th and  $j$ th fiducial points in the image plane, then iterating Eq. (8) with the simple update rule

$$\mathbf{s}(t + \Delta t) = \mathbf{s}(t) + \Delta t J^{-1}(\mathbf{s}(t))\mathbf{w}(t),$$

converges to the solution as long as  $\det(J) \neq 0$  and  $\|\mathbf{w}\|$  is small for all values of  $\mathbf{s}$  encountered during the iterations.

This method can be extended with a slight modification to cases where more than three lines are involved. For instance, if  $n$  lines are considered,  $n(n-1)/2$  constraint equations are obtained in the form of Eq. (6). The update rule in this case is

$$\mathbf{s}(t + \Delta t) = \mathbf{s}(t) + \Delta t (J^T J)^{-1} J^T \mathbf{w}(t).$$

The execution of this method with a number of different input data can be used to generate a look-up table that contains the values of  $\mathbf{s}$  corresponding to each set of input data, which are  $d_{12}$ ,  $d_{23}$ , and  $d_{13}$ . With the use of the table, there is no need to perform the computations in real time. Equally spaced values of  $d_{12}$ ,  $d_{23}$ , and  $d_{13}$  are generated first, and the computations are executed off line to obtain the values of  $\mathbf{s}$ . Given measured values of  $d_{12}$ ,  $d_{23}$ , and  $d_{13}$ , the corresponding values of  $\mathbf{s}$  can be interpolated from the look-up table.

This look-up table method was implemented by using three-dimensional linear interpolation that is essentially the three-dimensional extension of the following equation of one-dimensional linear interpolation:

$$f(u) = \frac{f(u_2) - f(u_1)}{u_2 - u_1} (u - u_1) + f(u_1).$$

Due to limited disk space and time for the generation of the table, a  $50 \times 50 \times 50$  table was used. However, this method did not show any advantage in speed over the on-line computation method, despite a very small table size. Thus we omitted this method from further tests in Sec. IV.

## 2. Determination of rigid-body motion

After obtaining the arclength of lines using methods described in the previous section, it remains for us to determine the rigid-body motion of a frame fixed to the image plane relative to the space-fixed reference frame. We assume here that the correspondence between points in the two-point sets has been established *a priori*, and we seek to find the relative rigid-body motion that will best match the two sets of points in the sense of least squared error. This is what we call the static rigid-body motion estimation problem with *a priori* correspondence.<sup>15-17</sup> In the context of computer vision and image analysis, many other related pose determination/estimation problems have been studied extensively.<sup>18-21</sup>

Consider two sets of  $n$  points in  $\mathbb{R}^3$  denoted as  $\{\mathbf{x}_i\}$  and  $\{\mathbf{y}_i\}$ . Here  $\{\mathbf{x}_i\}$  is a set of intersection points with respect to the space-fixed reference frame and  $\{\mathbf{y}_i\}$  describe the same points with respect to the frame fixed in the image plane, and the correspondence  $\mathbf{x}_i \leftrightarrow \mathbf{y}_i$  is assumed for all  $i = 1, \dots, n$ .

The goal is to find the rigid-body motion  $(R, \mathbf{b})$  such that  $\{\mathbf{y}_i\}$  is moved to fit in the “best” way to  $\{\mathbf{x}_i\}$ . One way to define the best fit is as the minimization of the weighted mean-square error,

$$E^2(R, \mathbf{b}) = \sum_{i=1}^n w_i \|\mathbf{x}_i - (R\mathbf{y}_i + \mathbf{b})\|^2. \tag{9}$$

The weights  $w_i$  satisfy  $w_i > 0$  and  $\sum_{i=1}^n w_i = 1$ , and were set to be equal to  $1/n$  in our computer implementation.

Note that this problem can be stated as not only a general three-dimensional (3-D)–3-D pose estimation but a simple 2-D–2-D pose estimation because we know in advance all the  $n$  points exist in a plane. However, solving the 2-D–2-D pose estimation problem requires another coordinate frame on the image plane and the relative rigid-body motion between the new frame and space-fixed reference frame is assumed already established. We review here Haralick’s approach of rigid-body motion for the 3-D–3-D pose estimation problem.<sup>20</sup>

Rewriting Eq. (9) with the constraint  $R^T R = I$  using Lagrangian multipliers results in

$$E^2(R, \mathbf{b}) = \sum_{i=1}^n \sum_{j=1}^3 w_i (x_{ij} - \mathbf{r}_j^T \mathbf{y}_i - b_j)^2 + \sum_{j=1}^3 \lambda_j (\mathbf{r}_j^T \mathbf{r}_j - 1) + 2\lambda_4 \mathbf{r}_1^T \mathbf{r}_2 + 2\lambda_5 \mathbf{r}_1^T \mathbf{r}_3 + 2\lambda_6 \mathbf{r}_2^T \mathbf{r}_3, \tag{10}$$

where  $\mathbf{x}_i = [x_{i1}, x_{i2}, x_{i3}]^T$ ,  $R = [\mathbf{r}_1, \mathbf{r}_2, \mathbf{r}_3]$ ,  $\mathbf{b} = [b_1, b_2, b_3]^T$ , and  $\lambda_1, \dots, \lambda_6$  are the Lagrangian multipliers.

Taking the partial derivatives of  $E^2(R, \mathbf{b})$  in Eq. (10) with respect to each component of  $\mathbf{b}$  and setting the derivatives to zero yields

$$\sum_{i=1}^n w_i (\mathbf{x}_i - R\mathbf{y}_i - \mathbf{b}) = 0.$$

By defining

$$\bar{\mathbf{x}} = \frac{\sum_{i=1}^n w_i \mathbf{x}_i}{\sum_{i=1}^n w_i}, \quad \bar{\mathbf{y}} = \frac{\sum_{i=1}^n w_i \mathbf{y}_i}{\sum_{i=1}^n w_i},$$

the translation vector,  $\mathbf{b}$ , is obtained:

$$\mathbf{b} = \bar{\mathbf{x}} - R\bar{\mathbf{y}}. \quad (11)$$

After substituting Eq. (11) into Eq. (10), we take the partial derivatives of  $E^2(R, \mathbf{b})$  with respect to the components of each  $\mathbf{r}_i$  and set the partial derivatives to zero. By rearranging the results and defining

$$A = \sum_{i=1}^n (\mathbf{y}_i - \bar{\mathbf{y}})(\mathbf{y}_i - \bar{\mathbf{y}})^T, \quad \Lambda = \begin{pmatrix} \lambda_1 & \lambda_4 & \lambda_5 \\ \lambda_4 & \lambda_2 & \lambda_6 \\ \lambda_5 & \lambda_6 & \lambda_3 \end{pmatrix},$$

and  $B = [\mathbf{b}_1, \mathbf{b}_2, \mathbf{b}_3]$ , where  $\mathbf{b}_j = \sum_{i=1}^n w_i (x_{ij} - \bar{x}_j)(\mathbf{y}_i - \bar{\mathbf{y}})$ ,  $\bar{x}_j = \sum_{i=1}^n w_i x_{ij} / \sum_{i=1}^n w_i$ , an equation,

$$AR^T + R^T \Lambda = B,$$

is acquired.

By observing that  $RB$  is symmetric and taking the singular value decomposition of  $B$ , i.e.,  $B = USV^T$ , the solution for the rotation matrix,  $R$ , is obtained:

$$R = VU^T. \quad (12)$$

Applying Eq. (12) to Eq. (11) yields the translation vector,  $\mathbf{b}$ .

## B. Minimization over position and orientation (Algorithms 2a and 2b)

The goal here is to determine the rigid-body motion that will place a frame of reference attached to the plane in such a way that the fiducial points are made to come as close as possible to the lines in space from which they arose.

Given the line defined by the position  $\mathbf{p}$  and unit direction vector  $\mathbf{v}$ , and given a point in space  $\mathbf{x}$ , we calculate the Euclidean distance between the line and point by minimizing the cost function,

$$c(s) = \|\mathbf{p} + s\mathbf{v} - \mathbf{x}\|^2 = \|\mathbf{p} - \mathbf{x}\|^2 + 2s\mathbf{v} \cdot (\mathbf{p} - \mathbf{x}) + s^2.$$

Setting  $dc/ds = 0$ , we see that the minimizing value of  $s$  is  $s_{\min} = -\mathbf{v} \cdot (\mathbf{p} - \mathbf{x})$ , and so the vector pointing from  $\mathbf{x}$  to the closest point on the line is

$$\mathbf{h} = (\mathbf{p} - \mathbf{x}) - [\mathbf{v} \cdot (\mathbf{p} - \mathbf{x})]\mathbf{v},$$

which we can write as

$$\mathbf{h} = (\mathbf{p} - \mathbf{x}) - \mathbf{v}\mathbf{v}^T(\mathbf{p} - \mathbf{x}) = (I - \mathbf{v}\mathbf{v}^T)(\mathbf{p} - \mathbf{x}).$$

Given  $n$  lines, we can then seek to minimize the cost function,

$$C(R, \mathbf{b}) = \sum_{i=1}^n \|(I - \mathbf{v}_i \mathbf{v}_i^T)(\mathbf{p}_i - \mathbf{x}_i)\|^2, \quad (13)$$

where

$$\mathbf{x}_i = R\mathbf{y}_i + \mathbf{b},$$

and  $\mathbf{y}_i$  is the position vector of the  $i$ th fiducial point relative to a frame fixed to the image plane. Whereas Haralick's method could be used to solve for  $R$  and  $\mathbf{b}$  in Eq. (9), it cannot be directly applied to Eq. (13). Hence, we use the methods of Sec. II B.

## 1. Gradient descent (algorithm 2a)

The cost function defined in Eq. (13) is a function of rigid-body motion, i.e., a rotation matrix,  $R$ , and a translation vector,  $\mathbf{b}$ . By employing a  $4 \times 4$  homogeneous transformation matrix,

$$H(R, \mathbf{b}) = \begin{pmatrix} R & \mathbf{b} \\ \mathbf{0}^T & 1 \end{pmatrix},$$

the cost function  $C(R, \mathbf{b})$  can be denoted as a function of  $H$ , i.e.,  $f(H)$ .

The cost function, Eq. (13), can be rewritten as

$$\begin{aligned} f(H) &\triangleq C(R, \mathbf{b}) \\ &= \sum_{i=1}^n \|(I - \mathbf{v}_i \mathbf{v}_i^T)(\mathbf{p}_i - \mathbf{x}_i)\|^2 \\ &= \sum_{i=1}^n \|(I - \mathbf{v}_i \mathbf{v}_i^T)[\mathbf{p}_i - (R\mathbf{y}_i + \mathbf{b}_i)]\|^2 \\ &= \sum_{i=1}^n [\mathbf{p}_i^T (I - 2\mathbf{v}_i \mathbf{v}_i^T + \mathbf{v}_i \mathbf{v}_i^T \mathbf{v}_i \mathbf{v}_i^T) \mathbf{p}_i - 2\mathbf{p}_i^T (I - 2\mathbf{v}_i \mathbf{v}_i^T \\ &\quad + \mathbf{v}_i \mathbf{v}_i^T \mathbf{v}_i \mathbf{v}_i^T) R\mathbf{y}_i - 2\mathbf{p}_i^T (I - 2\mathbf{v}_i \mathbf{v}_i^T + \mathbf{v}_i \mathbf{v}_i^T \mathbf{v}_i \mathbf{v}_i^T) \mathbf{b} \\ &\quad + (R\mathbf{y}_i)^T (I - 2\mathbf{v}_i \mathbf{v}_i^T + \mathbf{v}_i \mathbf{v}_i^T \mathbf{v}_i \mathbf{v}_i^T) R\mathbf{y}_i + 2(R\mathbf{y}_i)^T (I \\ &\quad - 2\mathbf{v}_i \mathbf{v}_i^T + \mathbf{v}_i \mathbf{v}_i^T \mathbf{v}_i \mathbf{v}_i^T) \mathbf{b} + \mathbf{b}^T (I - 2\mathbf{v}_i \mathbf{v}_i^T + \mathbf{v}_i \mathbf{v}_i^T \mathbf{v}_i \mathbf{v}_i^T) \mathbf{b}]. \end{aligned}$$

Defining

$$H \cdot (I + \epsilon \tilde{E}_i) = \begin{pmatrix} S & \mathbf{c} \\ \mathbf{0}^T & 1 \end{pmatrix},$$

$R$  and  $\mathbf{b}$  in the expression for  $f(H)$  are replaced by  $S$  and  $\mathbf{c}$ , respectively, as  $f(H(I + \epsilon \tilde{E}_i))$ . As described in Sec. II B, the minimum is reached by calculating the differential operators and updating  $H$ .

## 2. Partial closed-form analytical solution followed by gradient descent (algorithm 2b)

The algorithm explained in Sec. III B can be simplified by solving either  $\bar{X}_i^R f(H) = 0$  or  $\bar{X}_i^L f(H) = 0$  for  $i = 4, 5, 6$  for the three components of translation vector,  $\mathbf{b}$ .

For example, combining equations  $\bar{X}_i^L f(H) = 0$  for  $i = 4, 5, 6$  yields the following equation:

$$\sum_{i=1}^n (\mathbf{b} + R\mathbf{y}_i - \mathbf{p}_i)^T (I - 2\mathbf{v}_i \mathbf{v}_i^T + \mathbf{v}_i \mathbf{v}_i^T \mathbf{v}_i \mathbf{v}_i^T) = \mathbf{0}^T.$$

If we solve this equation for  $\mathbf{b}$ , we obtain

$$\begin{aligned} \mathbf{b} &= \left[ \sum_{i=1}^n (I - 2\mathbf{v}_i \mathbf{v}_i^T + \mathbf{v}_i \mathbf{v}_i^T \mathbf{v}_i \mathbf{v}_i^T) \right]^{-1} \\ &\quad \times \left[ \sum_{i=1}^n (I - 2\mathbf{v}_i \mathbf{v}_i^T + \mathbf{v}_i \mathbf{v}_i^T \mathbf{v}_i \mathbf{v}_i^T) (\mathbf{p}_i - R\mathbf{y}_i) \right]. \end{aligned} \quad (14)$$

Since  $\mathbf{b}$  is determined in Eq. (14) as a function of rotation parameters, the gradient descent method can be done on  $SO(3)$  rather than  $SE(3)$  with three parameters instead of six parameters. Hence, faster execution of the algorithm can be expected.

### C. Rate linearization of position and orientation (algorithm 3)

Instead of minimizing a scalar cost function with respect to rigid-body motion, we can formulate the problem as finding the rigid-body trajectory  $(R(t), \mathbf{b}(t))$  such that  $\mathbf{x}_i(t) = R(t)\mathbf{y}_i + \mathbf{b}(t)$  drives each of the vectors,

$$[I - \mathbf{v}_i \mathbf{v}_i^T](\mathbf{p}_i - \mathbf{x}_i(t)) = \hat{\mathbf{d}}_i(t), \quad (15)$$

to zero, where  $\mathbf{y}_i$  denotes the coordinates of the  $i$ th fiducial in the image plane. If this can be accomplished, it means that each of the fiducial marks is driven to its corresponding rod of the three-dimensional stereotactic frame.

Note that the matrix  $[I - \mathbf{v}\mathbf{v}^T]$  is not invertible since  $\|\mathbf{v}\|=1$  implies that the matrix  $\mathbf{v}\mathbf{v}^T$  has an eigenvalue equal to unity, which corresponds to eigenvector  $\mathbf{v}$ . Making the substitution  $\mathbf{x}_i(t) = R(t)\mathbf{y}_i + \mathbf{b}(t)$  in Eq. (15) and rearranging terms, we see that

$$[I - \mathbf{v}_i \mathbf{v}_i^T]\mathbf{p}_i - [I - \mathbf{v}_i \mathbf{v}_i^T](R\mathbf{y}_i + \mathbf{b}) = \hat{\mathbf{d}}_i(t).$$

We now take the derivative of both sides with respect to artificial time, and observe that  $\mathbf{p}_i$  and  $\mathbf{v}_i$  are constant vectors. If, in addition, we observe that

$$\dot{R}\mathbf{y}_i = \dot{R}R^T R\mathbf{y}_i = \boldsymbol{\omega} \times (R\mathbf{y}_i) = -(R\mathbf{y}_i) \times \boldsymbol{\omega},$$

where  $\boldsymbol{\omega} = \text{vect}(\dot{R}R^T)$ , then we can write the time derivative of Eq. (15) as

$$[I - \mathbf{v}_i \mathbf{v}_i^T][\text{matr}(R\mathbf{y}_i), -I][\boldsymbol{\omega}^T, \dot{\mathbf{b}}^T]^T = \dot{\hat{\mathbf{d}}}_i. \quad (16)$$

Here we use the notation  $\mathbf{n} = \text{vect}(N)$  and  $N = \text{matr}(\mathbf{n})$  if  $N$  is the skew-symmetric matrix such that  $N\mathbf{x} = \mathbf{n} \times \mathbf{x}$  for every  $\mathbf{x} \in \mathbb{R}^3$ . We have also used the fact that  $\dot{R}R^T$  is always skew symmetric when  $R \in SO(3)$ .<sup>14</sup>

If we force  $\hat{\mathbf{d}}_i$  to zero by defining

$$\dot{\hat{\mathbf{d}}}_i = -\alpha \hat{\mathbf{d}}_i,$$

for some positive constant  $\alpha$ , then  $\boldsymbol{\omega}$  and  $\dot{\mathbf{b}}$  can be solved for at each value of time along the way by inverting the over-constrained system resulting from concatenating Eq. (16) for  $i = 1, 2, \dots, n$ . Once this is done, the values of  $\mathbf{b}(t)$  and  $R(t)$  can be updated using the rules

$$\mathbf{b}(t + \Delta t) = \mathbf{b}(t) + \Delta \dot{\mathbf{b}}(t)$$

and

$$R(t + \Delta t) = [I + \Delta t \text{matr}(\boldsymbol{\omega}(t))]R(t).$$

Since the rotational updates have the potential to cause  $R(t)$  to stray from being a rotation matrix, the occasional renormalization,

$$R(t) \rightarrow R(t)(R^T(t)R(t))^{-1/2},$$

may be required. This step could be replaced by finding the Euler angles or Cayley parameters that best approximate  $R(t)$ , then replace  $R(t)$  with the resulting rotation matrix.

We note that if the actual rotation matrix is close to being the identity matrix (as will be the case when the image plane is close to cutting the cage straight on), then only one iteration may be required.

### D. Minimization over position, orientation, and arclengths (algorithm 4)

Given the coordinates  $\{\mathbf{y}_i\}$  of fiducials in the image plane, we can simultaneously solve for the position and orientation of a reference frame attached to the image plane and the arclengths  $\{s_i\}$  as follows:

We observe that

$$\mathbf{p}_i + s_i \mathbf{v}_i = R\mathbf{y}_i + \mathbf{b}. \quad (17)$$

Let us assume that we have an initial guess for the orientation of the frame attached to the image plane, and that the actual orientation is not very different than this initial guess. Then we write

$$R = R_0(I + \Omega).$$

Here  $\Omega = -\Omega^T$  has entries that are small. The vector  $\boldsymbol{\omega}$  is defined, such that

$$\boldsymbol{\omega} \times \mathbf{x} = \Omega \mathbf{x},$$

for any  $\mathbf{x} \in \mathbb{R}^3$ . This means we can rewrite Eq. (17) as

$$\mathbf{p}_i - s_i \mathbf{v}_i + R_0 \mathbf{y}_i - R_0(\mathbf{y}_i \times \boldsymbol{\omega}) + \mathbf{b}.$$

By defining  $Y_i$  to be the matrix such that  $Y_i \mathbf{x} = \mathbf{y}_i \times \mathbf{x}$  for every  $\mathbf{x} \in \mathbb{R}^3$ , it follows that we can write the following linear equation:

$$\mathbf{p}_i - R_0 \mathbf{y}_i = [\mathbf{0}, \dots, \mathbf{0}, -\mathbf{v}_i, \mathbf{0}, \dots, \mathbf{0}, -R_0 Y_i, I] \begin{bmatrix} s \\ \boldsymbol{\omega} \\ \mathbf{b} \end{bmatrix},$$

where

$$\mathbf{s} = [s_1, \dots, s_i, \dots, s_n]^T.$$

Stacking these equations on top of each other for  $i = 1, \dots, n$  results in a system of  $(3n) \times (n+6)$  scalar equations in  $n+6$  parameters ( $n$  arclengths and 6 rigid-body motion parameters). This can be solved in the least-squares sense using a pseudoinverse.

## IV. EXPERIMENTAL RESULTS AND DISCUSSION

The algorithms described in the previous section were implemented in Matlab. The input data to the algorithms are 2-D coordinates of the centroids of fiducial marks, as they are found in a cross-sectional image. The algorithms assume that the image already has been processed, and hence the centroid locations of fiducial marks have been extracted and matched with the rods. The image processing software typically has *a priori* knowledge of the gross initial orientation and the geometric description of the fiducial frame, which is usually sufficient for the determination of correspondence. In

difficult cases some operator input can be required, in the form of a few mouse clicks. Solving the correspondence problem as part of the numerical minimization would be more elegant, but would also require significantly more processing time. We will explore this option in future work.

In our experiments, we used actual patient data acquired in 1995 and 1996 on a General Electric CT Scanner at the George Washington University Hospital. For stereotactic registration Kelly and BRW head frames were used. The images were processed and contoured with a clinically commissioned stereotactic navigation system (GWST Linac Knife v5.2), which was developed and maintained at the George Washington University Hospital.

The locations of fiducial marks were determined in the following manner: The images were thresholded by setting the window and level parameters until all noise and artifacts disappeared from around the fiducial rods. In each image, a sufficiently large contour line around each fiducial mark was drawn such that it completely surrounded the fiducial mark with some black margin. Because of the prior thresholding, the pixel values in the black margin were guaranteed to be zero. The software calculated the centroid of the interior of the contour line, which was considered as the center of the fiducial mark. When the GWST Linac Knife system was commissioned, this function was also carefully tested on a large number of CT and MRI images and with various threshold settings. Background noise, when there was any, was effectively removed by simple thresholding. The typical pixel size in a stereotactic case was around 0.5 mm, the diameter of a fiducial rod was 5 mm, and each fiducial mark contained at least 75 pixels. This convinced us that the GWST Linac Knife system calculated the centroids of fiducial marks in a fairly consistent and accurate manner. Nevertheless, the quality of the input data was analyzed retrospectively.

Two sets of real CT data for the BRW frame (43 image slices each) and one set of real CT data for the Kelly frame (10 image slices) were used in our experiments. The image size and FOV (Field of View) for both the BRW and Kelly frames were 512×512 pixels and 34.5 mm, respectively. The thickness of image slices was 3 mm for the BRW frame 5 mm for the Kelly frame.

In each clinical case, a series of consecutive slices were acquired. The head of the patient (with the head frame on) was fixed firmly to the scanner bed. Consequently, the locations of a given fiducial rod found in the full series must fit a straight line and the extent of deviation from this line is a good measure of the “noisiness” of our input data. The av-

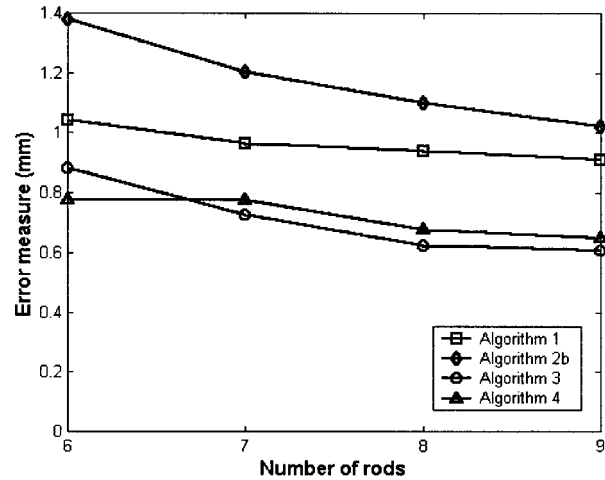


Fig. 6. Error measures defined in Eq. (18) are displayed for each algorithm. The input was synthetic data with 0.2 mm amplitude of noise.

erage deviation in the Kelly frame data was 0.097 mm and the average deviations in the two sets of BRW frame data were 0.267 and 0.111 mm. Therefore the average deviation of the real CT data was about 0.15 mm.

We also examined the sensitivity of our algorithms to “noise” added to fiducial locations. In addition to real CT data, 40 synthetic datasets were generated by transforming the reference frame from the identity. The synthetic data covered a large range of rigid-body motions, ±25° around each rotation axis. The case of zero noise represents ideal input data, in which case the residual registration error originates solely from the algorithm and its implementation. The amplitude of noise was kept constant while its direction was randomized. All the algorithms were tested at six different noise amplitudes, from 0 to 0.5 mm with the increment of 0.1 mm. We also included simulated cases when fewer than all the fiducial rods were available for registration, and analyzed the combined effect of noise and missing fiducials.

In order to compare the resistance of the algorithms to noise, a distance metric on  $SE(3)$  (three-dimensional rigid-body motion group) was used. We applied a metric, which measures the error of a local frame  $g_2=(R_2, \mathbf{b}_2)$  from a reference frame  $g_1=(R_1, \mathbf{b}_1)$  as<sup>14</sup>

$$d_{SE(3)}^{(2)}(g_1, g_2) = \sqrt{L^2(d_{SO(3)}(R_1, R_2))^2 + (d_{R^3}(\mathbf{b}_1, \mathbf{b}_2))^2}, \tag{18}$$

where  $d_{SO(3)}(R_1, R_2) = \sqrt{6 - 2 \text{trace}(R_1^T R_2)}$  is a distance metric on  $SO(3)$  (the three-dimensional rotation group) and

TABLE I. Error measures (mm) of algorithms for synthetic data with 0.2 mm noise.

| Algorithms | 6 rods | 7 rods | 8 rods | 9 rods |
|------------|--------|--------|--------|--------|
| 1          | 1.0423 | 0.9664 | 0.9394 | 0.9130 |
| 2b         | 1.3813 | 1.2023 | 1.0983 | 1.0243 |
| 3          | 0.8834 | 0.7284 | 0.6255 | 0.6095 |
| 4          | 0.7774 | 0.7754 | 0.6754 | 0.6494 |

TABLE II. Error measures (mm) of algorithms for synthetic data with 0.5 mm noise.

| Algorithms | 6 rods | 7 rods | 8 rods | 9 rods |
|------------|--------|--------|--------|--------|
| 1          | 3.6891 | 2.6835 | 2.5864 | 1.9823 |
| 2b         | 1.7523 | 1.6563 | 1.5994 | 1.5733 |
| 3          | 1.9784 | 1.8924 | 1.7714 | 1.7044 |
| 4          | 1.9744 | 1.7764 | 1.6424 | 1.6254 |

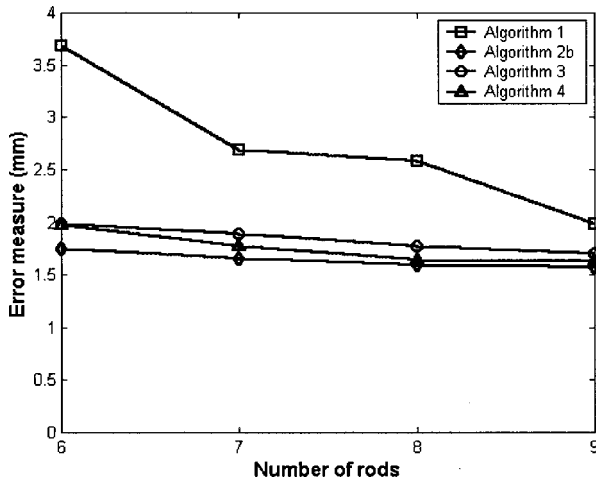


FIG. 7. Error measures defined in Eq. (18) are displayed for each algorithm. The input was synthetic data with 0.5 mm amplitude of noise.

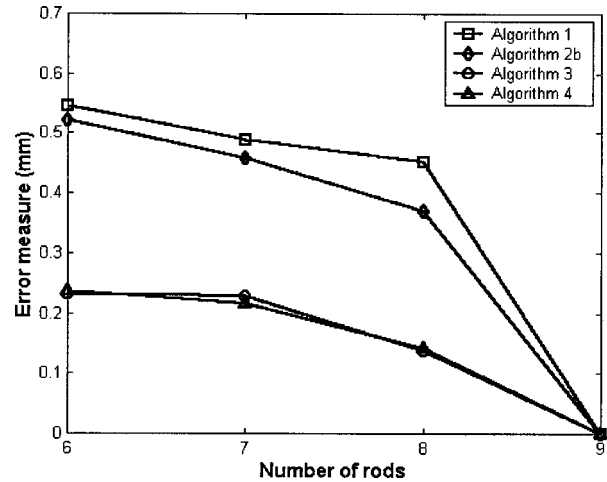


FIG. 8. Error measures defined in Eq. (18) are displayed for each algorithm. The input was real CT data.

$d_{R^3}(\mathbf{b}_1, \mathbf{b}_2) = \|\mathbf{b}_1 - \mathbf{b}_2\|$  is the Euclidean distance between points  $\mathbf{b}_1$  and  $\mathbf{b}_2$ . Here  $L$  is a measure of length that makes the units of orientational and translational displacements compatible. The radius of a fiducial rod, 2.5 mm, was used for this value. Other suitable error metrics have also been discussed by Park<sup>22</sup>, and Chirikjian and Zhou.<sup>23</sup>

Table I and Fig. 6 display the error measures for synthetic data with 0.2 mm amplitude of noise for each algorithm. Table II and Fig. 7 also show the error measures for synthetic data but the amplitude of noise is 0.5 mm. The reason for selecting 0.2 and 0.5 mm for the amplitude of noise is that the average deviation in the real CT data is about 0.15 mm and the amplitude of 0.5 mm is considered to be an extreme case. Here the reference frame  $g_1$  in Eq. (18) is the frame in the case of synthetic data with zero noise.

When 0.2 mm noise was applied, Algorithm 3 (rate linearization of position and orientation) and algorithm 4 (minimization over position, orientation, and arclengths) outperformed algorithm 1 (solving a system of polynomials) and algorithm 2b (gradient descent method with partial closed-form solution). Since algorithm 2b runs faster than algorithm 2a, only numerical results with algorithm 2b are listed in tables and figures. When 0.5 mm noise was applied, algorithm 2b was found to be the best performing method. However, its advantage over algorithms 3 and 4 is not significant. Considering that 0.2 mm noise is close to the noise in the real data, algorithms 3 and 4 are the least sensitive methods to realistic noise.

Table III and Fig. 8 show the error measures for the real CT data for each algorithm. In this experiment, the reference

frame  $g_1$  in Eq. (18) is the frame in the case of complete data (nine rods). As a result of this test, algorithms 3 and 4 are the most robust to missing fiducials. Table III also indicates that algorithm 1 is the most sensitive to missing fiducials in real CT data. However, note that the distance measure in the worst case (algorithm 1 with 6 rods only) is still only about 1 pixel (0.5 mm). The robustness of the algorithms to missing fiducials is also observed in Tables I and II, except algorithm 1 for 0.5 mm noise.

Table IV and Fig. 9 display the running speed of the algorithms for the real CT data. The speed was measured first in FLOPs (Floating Point Operations) and then was normalized to the value of the fastest case, which was found to be algorithm 4 with 6 rods. Algorithm 4 outperforms other algorithms. Algorithm 2b is the slowest method because the convergence needs a significant number of iterations. The average running time of algorithm 4 for real CT data with 6 rods was 0.3236 s in a Matlab implementation on a Windows PC with a Pentium II 366 MHz processor and 64 MB RAM.

Algorithms 2b, 3, and 4 require the rotation matrix to be initialized before starting iteration. Hence, the sensitivity of those algorithms to initial guesses was also investigated. Thirty initial rotation matrices were generated for simulations in a similar way the synthetic input data was generated. Ten rotation angles from  $-50^\circ$  to  $+50^\circ$  with the increment of 10 were selected, and then three rotation axes were combined. It was observed that algorithm 4 is not affected by the initial rotation matrix. The influence of the initial guess on algorithms 2b and 3 is negligible if the rotation angle is in

TABLE III. Error measures (mm) of algorithms for real CT data.

| Algorithms | 6 rods | 7 rods | 8 rods | 9 rods |
|------------|--------|--------|--------|--------|
| 1          | 0.5454 | 0.4889 | 0.4515 | 0.0    |
| 2b         | 0.5218 | 0.4569 | 0.3693 | 0.0    |
| 3          | 0.2323 | 0.2285 | 0.1384 | 0.0    |
| 4          | 0.2369 | 0.2150 | 0.1413 | 0.0    |

TABLE IV. Speed of algorithms for real CT data (normalized to the fastest case, algorithm 4 with 6 rods).

| Algorithms | 6 rods  | 7 rods   | 8 rods   | 9 rods   |
|------------|---------|----------|----------|----------|
| 1          | 2.0949  | 3.9164   | 5.8671   | 7.9421   |
| 2b         | 80.1786 | 143.5839 | 176.7634 | 199.9542 |
| 3          | 4.5768  | 7.3586   | 8.8758   | 10.5977  |
| 4          | 1.0000  | 1.2335   | 1.5577   | 1.8806   |

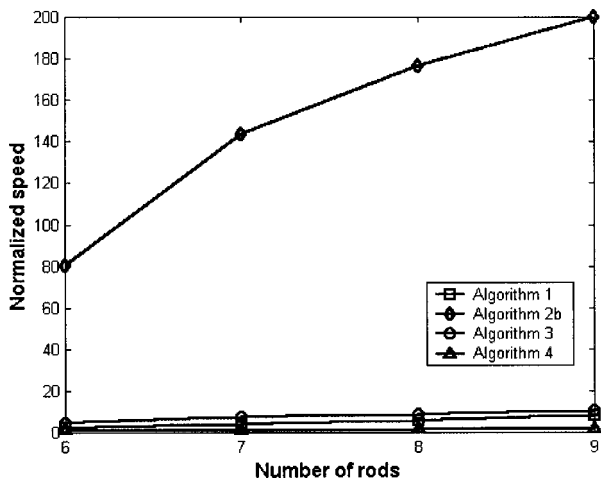


FIG. 9. The running speed of each algorithm is displayed with the number of rods. Results were normalized to the fastest case, which is algorithm 4 with 6 rods.

the range of  $[-20, 20]^\circ$ . Therefore, the identity matrix can be recommended for the initial rotation matrix. Note that in most clinical cases, we try to align the patient close to that orientation.

All experiments considered, algorithm 4 performed the best among the four methods. Algorithm 3 is our second best.

## V. CONCLUSIONS

In this paper, we presented two families of numerical algorithms for registration of rigid line fiducial objects to their marks in cross-sectional planar images, such as CT or MRI. We demonstrated the methods in actual CT data and in synthetic data simulating real-life noise. Two broad categories of algorithms were discussed: (1) methods that first seek the parameters describing the image plane, and then register within that plane; and (2) methods that register the planar points to the three-dimensional fiducials directly. The two best performing algorithms, algorithms 3 and 4, both belong to the second category.

An important strength of these numerical methods is the ability to handle incomplete fiducial patterns. They are sufficiently robust to handle as few as six fiducials out of nine, in contrast to traditional registration methods that require the presence of all nine fiducial rods. Theoretically only as few as three nonparallel fiducial rods should be sufficient for registration. Our future work will include tests of our algorithms in such extreme cases.

Another strength of our algorithms is their applicability to an arbitrary combination of line fiducial patterns without requiring modification of the algorithm. For example, we ran the same registration programs for BRW and Kelly stereotactic head frames, without any algorithmic modification. The geometrical definition of the individual fiducial rods was simply input data to our algorithms.

All tested algorithms (and not just the two winners) are resistant to noise in the input data. The running time of the algorithms is also affordable, even in intraoperative applica-

tions. The average running time of the fastest algorithm is 0.3236 s for six fiducial lines in real CT data in a Matlab implementation. The program was not optimized for speed.

The immediate field of use of these algorithms is frame-based stereotactic navigation, as applied in radiosurgery and functional neurosurgery. Perhaps even more importantly, the algorithms appear to be applicable in problems where dexterous robotic end-effectors need to be registered to CT images in an intraoperative scenario. Currently, there is a comprehensive research program at the Johns Hopkins University in robotically assisted needle placement, with a current focus on prostate,<sup>8</sup> spine,<sup>9,11,13</sup> and kidney<sup>11</sup> applications. We will be implementing and testing the performance of our registration methods in clinical test bed applications in the near future.

## ACKNOWLEDGMENTS

The authors would like to thank Attila Tanacs and Haesung Yu for providing some of the figures in this paper. This work was supported in part by the National Science Foundation under the Engineering Research Center grant No. EEC9731478 and by a United Engineering Foundation grant.

<sup>a</sup>Electronic mail: gregc@jhu.edu

<sup>1</sup>R. A. Brown, T. S. Roberts, and A. G. Osborne, "Stereotactic frame and computer software for CT-directed neurosurgical localization," *Invest. Radiol.* **15**, 308–312 (1980).

<sup>2</sup>S. Goerss, P. J. Kelly, B. Kall, and G. J. Alker, "A computed tomographic stereotactic adaptation system," *Neurosurgery* **10**, 375–379 (1982).

<sup>3</sup>L. Leksell and B. Jerenberg, "Stereotaxis and tomography: a technical note," *Acta Neurochir* **52**, 1–7 (1980).

<sup>4</sup>I. Lax, H. Blomgren, I. Nasrund, and R. Svanstrom, "Stereotactic radiotherapy of malignancies in the abdomen. Methodological aspects," *Acta Oncol.* **33**, 677–683 (1994).

<sup>5</sup>I. Takacs and A. J. Hamilton, "Extracranial stereotactic radiosurgery: applications for the spine and beyond," *Neurosurg. Clin. N. Am.* **10**, 257–270 (1999).

<sup>6</sup>F. Lohr *et al.*, "Noninvasive patient fixation for extracranial stereotactic radiotherapy," *Int. J. Radiat. Oncol., Biol., Phys.* **45**, 521–527 (1999).

<sup>7</sup>Y. E. Erdi *et al.*, "A new fiducial alignment system to overlay abdominal CT or MR anatomical images with radiolabeled antibody SPECT scans," *Cancer* **73**, 923–931 (1994).

<sup>8</sup>G. Fichtinger, T. L. DeWeese, A. Patriciu, A. Tanacs, D. Mazilu, J. H. Anderson, K. Masamune, R. H. Taylor, and D. Stoianovici, "Robotically assisted prostate biopsy and therapy with intra-operative CT guidance," *J. Acad. Radiol.* **9**, 60–74 (2002).

<sup>9</sup>K. Masamune *et al.*, "System for robotically assisted percutaneous procedures with computed tomography guidance," *J. Computer Assisted Surgery* **6**, 370–383 (2001).

<sup>10</sup>R. Susil, J. Anderson, and R. Taylor, "A single image registration method for CT guided interventions," *Proceedings to MICCAI 1999*, Lecture Notes in Computer Science (Springer-Verlag, Berlin, 1999), Vol. 1679, pp. 798–808.

<sup>11</sup>A. Patriciu, S. Solomon, L. Kavoussi, and D. Stoianovici, "Robotic kidney and spine percutaneous procedures using a new laser-based CT registration method," *Proceedings to MICCAI 2001*, Lecture Notes in Computer Science (Springer-Verlag, Berlin, 2001), Vol. 2208, pp. 249–257.

<sup>12</sup>W. Zylka, J. Sabczynski, and G. Schmitz, "A Gaussian approach for the calculation of the accuracy of stereotactic frame systems," *Med. Phys.* **26**, 381–391 (1999).

<sup>13</sup>K. Cleary, S. Onda, F. Banovac, D. Lindisch, N. Glossop, L. Jiang, S. Xu, A. Patriciu, and D. Stoianovici, "CT-guided robotic biopsy testbed: user interface and coordinate transformations," *Proceedings of Computer Assisted Radiology and Surgery* (Elsevier, Amsterdam, 2001), pp. 171–177.

- <sup>14</sup>G. S. Chirikjian and A. B. Kyatkin, *Engineering Applications of Noncommutative Harmonic Analysis* (CRC, Boca Raton, FL, 2000).
- <sup>15</sup>K. S. Arun, T. S. Huang, and S. D. Blostein, "Least-squares fitting of two 3-D point sets," *IEEE Trans. Pattern Anal. Machine Intelligence* **9**, 698–700 (1987).
- <sup>16</sup>A. Nádás, "Least squares and maximum likelihood estimates of rigid motion," IBM Research Report, RC 6945 (#29783), Mathematics, 17 January 1978.
- <sup>17</sup>S. Umeyama, "Least-squares estimation of transformation parameters between two point patterns," *IEEE Trans. Pattern Anal. Mach. Intell.* **13**, 376–380 (1991).
- <sup>18</sup>D. W. Eggert, A. Lorusso, and R. B. Fischer, "Estimating 3-D rigid body transformations: A comparison of four major algorithms," *Mach. Vision Appl.* **9**, 272–290 (1997).
- <sup>19</sup>D. Goryn and S. Hein, "On the estimation of rigid-body rotation from noisy data," *IEEE Trans. Pattern Anal. Mach. Intell.* **17**, 1219–1220 (1995).
- <sup>20</sup>R. M. Haralick *et al.*, "Pose estimation from corresponding point data," *IEEE Trans. Syst. Man Cybern.* **19**, 1426–1446 (1989).
- <sup>21</sup>P. L. Rosin, "Robust pose estimation," *IEEE Trans. Syst. Man Cybern.* **29**, 297–303 (1999).
- <sup>22</sup>F. C. Park, "Distance metrics on the rigid-body motions with applications to mechanism design," *Int. J. Robot. Res.* **117**, 36–40 (1994).
- <sup>23</sup>G. S. Chirikjian and S. Zhou, "Metrics on motion and deformation of solid models," *J. Mech. Des.* **120**, 252–261 (1998).